Predicting Steady Shear Rheology of Condensed-Phase Monomolecular Films at the Air-Water Interface

Aditya Raghunandan and Amir H. Hirsa
Department of Mechanical, Aerospace and Nuclear Engineering, Rensselaer Polytechnic Institute, Troy, New York 12180-3590, USA

Patrick T. Underhill
Department of Chemical and Biological Engineering, Rensselaer Polytechnic Institute, Troy, New York 12180-3590, USA

Juan M. Lopez*
School of Mathematical and Statistical Sciences, Arizona State University, Tempe, Arizona 85287, USA

(Received 30 March 2018; revised manuscript received 30 May 2018; published 17 October 2018)

Predicting the non-Newtonian shear response of soft interfaces in biophysical systems and engineered products has been compromised by the use of linear (Newtonian) constitutive equations. We present a generalized constitutive equation, with tractable material properties, governing the response of Newtonian and non-Newtonian interfaces subjected to a wide range of steady shear. With experiments spanning six decades of shear rate, we capture and unify divergent reports of shear-thinning behavior of monomolecular films of the lipid dipalmitoylphosphatidylcholine, the primary constituent of mammalian cell walls and lung surfactant, at near-physiological packing densities.

DOI: 10.1103/PhysRevLett.121.164502

Colloidal particles, proteins, and other surface-active materials such as phospholipids organize into a variety of multiphasic two-dimensional (2D) soft matter systems at fluid-fluid interfaces. Even under relatively small hydrodynamic stresses, the response of such systems is highly nonlinear [1]. Accounting for this nonlinear shear response is crucial to understanding many biophysical processes, including the role of natural surfactant systems in pulmonary flow [2] and the variable fluidity of mammalian cell walls that facilitates nutrient exchange while providing structural integrity to the cell [3]. Modeling and predicting the nonlinear interfacial shear response also has critical technological implications with interfacial rheology emerging as a paradigm for the design of controlled-release systems (microcapsules) and stabilizers that prevent emulsion dissolution, ensuring long shelf life of pharmaceuticals, cosmetics, and foods [4–6].

A significant body of work aimed at describing the rheology of these interfacial systems has been performed under conditions that minimize the nonlinear hydrodynamic effects associated with the coupling between the interfacial and bulk flow stresses. This requires either an infinite ratio of surface viscosity to the product of bulk viscosity and a length scale, or a Stokes flow limit for the bulk where flow inertia is negligible. The consequences of these limits are that either the speed or oscillation of the shearing probe needs to be very small or using very small length scales [7–10]. In practice this restricts the upper limit of shear that can be imposed on the interface, and many condensed films cannot be sheared under these conditions.

Although rheological relationships have been established, prediction of flow behavior (especially under conditions that differ from those used to determine rheological properties) has yet to be demonstrated due to the lack of mechanistic models that can accurately predict the observed nonlinear interfacial responses across flow conditions and geometries [11]. Some studies quantify interfacial rheology at regimes where the bulk flow inertia is non-negligible, but implement a simple linear additive model to decompose the contributions from the interfacial and bulk stresses to the measured response [12,13].

Predicting interfacial shear response requires prescribing a constitutive equation for the interface. A constitutive equation consists of material properties of the 2D system, such as surface shear viscosity, which relate the imposed stresses to the observed interfacial shear. The simplest linear constitutive equation corresponding to a Newtonian interface is the Boussinesq-Scriven surface model [14]. For a purely shearing interfacial flow, where the effects of surface dilatational viscosity are absent, the Newtonian surface model becomes

$$\tilde{\boldsymbol{\tau}}^s = 2\mu^s \boldsymbol{D}^s, \tag{1}$$

where μ^s is the surface shear viscosity, a single parameter relating the surface stress tensor $\tilde{\boldsymbol{\tau}}^s$ to the surface rate of

deformation tensor $\boldsymbol{D}^s$. This model (or its viscoelastic generalizations) has been implemented to correlate measured torque [15] and rotational or translational drag [16] to the shear imposed locally, thereby determining the surface shear viscosity. The technique works well if the response is linear, with a single value of surface shear viscosity governing the interfacial response across flow conditions. However, shear thinning and other nonlinear (non-Newtonian) interfacial responses due to the presence of large macromolecules, such as proteins or densely packed condensed-phase monolayers of phospholipids, are also interpreted using this linear constitutive equation. Nonlinearity is inferred if the surface shear viscosity depends on the imposed shear rate. This has led to reports of "apparent" surface rheological properties that depend on the rate of deformation and the flow geometry, leading to inconsistent measurements and the inability to predict the response under different flow conditions [11].

In this Letter, we present a non-Newtonian constitutive equation for 2D soft matter systems under steady shear that is two-way coupled to the fully nonlinear bulk flow; i.e., the interfacial and the bulk flows are viscously coupled to each other. The 2D constitutive equation takes the Newtonian functional form, but the surface shear viscosity is generalized to be a function of the imposed shear rate. For shearing interfacial flows, the constitutive relation becomes

$$\tilde{\boldsymbol{\tau}}^s = 2\mu^s_{\mathrm{eff}}\boldsymbol{D}^s, \tag{2}$$

where μ^s_{eff} is the effective surface shear viscosity, a function of the magnitude of the local interfacial shear rate $\dot{\gamma}$. We demonstrate the applicability of this equation to determine the material properties that govern the nonlinear response of a model interfacial film in a canonical axisymmetric flow geometry.

Interfacial films of dipalmitoylphosphatidylcholine (DPPC) play a crucial role in human physiology and health. DPPC is the main constituent of pulmonary surfactant and the bilayer that forms cell-wall membranes. Monolayers of DPPC also serve as a model for the lipid layer that forms the outer portion of the tear film covering our eyes. The melting temperature of DPPC is approximately 41 °C; thus it predominantly exists in densely packed condensed phases in the body [17]. Such condensed-phase monolayers of DPPC also serve as models of a single leaflet of the cell membrane bilayer [18], with the molecular area of the phospholipids constituting the bilayer resembling a monolayer of DPPC at high surface pressures [19] ($\Pi > 15$ mN/m, where surface pressure Π is the reduction in surface tension of the monolayer-laden interface compared to a clean interface).

Our choice for the functional form of μ^s_{eff} is motivated by the multiple reports of shear-thinning in DPPC films at high surface packing (corresponding to large surface pressure $\Pi \gtrsim 30$ mN/m) and its Newtonian response at low packing ($\Pi < 15$ mN/m) [20–22], and is inspired by the Sisko model in bulk (3D) rheology [23]:

$$\mu^s_{\mathrm{eff}} = \mu^s_\infty + \tilde{K}|\dot{\gamma}|^{n-1}, \tag{3}$$

where μ^s_∞ is the surface shear viscosity at very large shear rates, $\tilde{K}$ is the consistency index, and n is the power-law index. μ^s_∞, $\tilde{K}$, and n are material properties of the interface, and as such are only functions of the thermodynamic state of the material at the interface, i.e., the surface pressure Π of the monolayer at a given temperature. In the limit $\tilde{K} \to 0$, one recovers the Newtonian constitutive equation, and the limit $n \to 1$ with $\tilde{K} \neq 0$ corresponds to a Bingham model incorporating a yield stress with a Newtonian excess stress behavior. To model a shear-thinning film with a yield stress, a term $\tilde{\tau}|\dot{\gamma}|^{-1}$ could be added to the right-hand side of Eq. (3), where $\tilde{\tau}$ is the yield stress of the monolayer. In the comparisons with the experiments presented below, we find that the interfacial film is shear thinning, so $\tilde{K} \neq 0$ and $n \neq 1$. A yield stress behavior could manifest at low enough shear rates but does not affect the comparisons nor the interpretation of the results for the range of shear rates presented here. As such, we keep Eq. (3) as it stands for ease of dissemination. The approach presented here is general, allowing for different forms of μ^s_{eff} to account for responses of steadily sheared films under various conditions, making Eq. (3) applicable across a range of interfacial packing densities (Π) of monolayers such as DPPC.

We chose the knife-edge flow geometry as the canonical axisymmetric system to examine how well Eq. (3) captures the non-Newtonian response of DPPC monolayers. A schematic of the knife-edge flow geometry is presented in Fig. 1. There are four associated length scales: a the knife-edge outer radius, aA_R the cylinder radius, aA_H the bulk liquid depth, and ϵa the knife-edge thickness. The knife-edge thickness ϵa is of secondary importance (established experimentally by Slattery [24]), as is the bulk liquid depth aA_H. The length scale of primary importance is the distance over which the interface is sheared, $a(A_R - 1)$. We nondimensionalize length with a. There are two time scales for the flow, which are independent of the monolayer: the knife-edge rotation time $1/\Omega$ and the bulk viscous diffusion time a^2/ν, where Ω is the angular velocity of the knife edge and ν is the kinematic viscosity of the (Newtonian) bulk phase. Their ratio is the Reynolds number $\mathrm{Re} = \Omega a^2/\nu$. We use $1/\Omega$ to nondimensionalize time. The nondimensional shear rate is defined as

$$S = (aA_R)^2\dot{\gamma}/\nu = A_R^2\mathrm{Re}(\partial v^s/\partial r - v^s/r), \tag{4}$$

where v^s is the azimuthal component of velocity at the air-water interface $z = A_H$. Of the three interfacial material properties, n is already dimensionless. The second, $\tilde{K}$, is nondimensionalized to K defined by

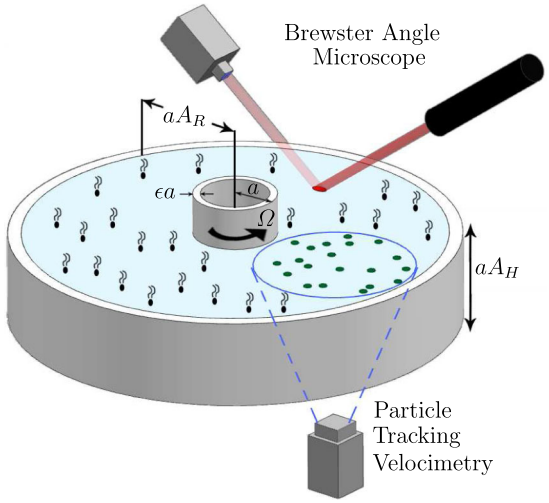

FIG. 1. Schematic of the knife-edge geometry, and the experimental setup.

$$K = [(aA_R)^2/\nu]^{(1-n)}\tilde{K}/\mu^s_\infty. \tag{5}$$

With these definitions, the effective viscosity in Eq. (3) is expressed as an effective Boussinesq number, $\mathrm{Bo}_{\mathrm{eff}}$,

$$\mathrm{Bo}_{\mathrm{eff}} = \mathrm{Bo}(1 + K|S|^{n-1}). \tag{6}$$

In Eq. (6), $\mathrm{Bo} = \mu^s_\infty/(\mu a)$ is the Boussinesq number, the third dimensionless interfacial material property, which is a ratio of surface to bulk phase stresses, and μ is the dynamic viscosity of the bulk phase liquid. The nondimensional azimuthal component of the interfacial stress balance [Eq. (2)] becomes

$$(1 + nK|S|^{n-1})\frac{\partial^2 v^s}{\partial r^2} + [1 + (2-n)K|S|^{n-1}] \times \left(\frac{1}{r}\frac{\partial v^s}{\partial r} - \frac{v^s}{r^2}\right) = \frac{1}{\mathrm{Bo}}\frac{\partial v}{\partial z}\bigg|_{z=A_H}. \tag{7}$$

Solving Eq. (7) gives $v^s = v|_{z=A_H}$, the nondimensional azimuthal velocity at the interface. However, Eq. (7) requires computing the normal gradient of v at the interface, $\partial v/\partial z|_{z=A_H}$, which is determined by simultaneously solving the Navier-Stokes equations for the bulk flow in the cylinder using Eq. (7) as the boundary condition at the interface. The numerics involved are detailed in Ref. [25]; a brief overview is presented in the Supplemental Material [26], which includes Refs. [8,20–22,25,27–29].

To test the effectiveness of this model, steady-shear experiments were conducted with DPPC monolayers spread on pure water at 23 °C, with $\nu = 9.33 \times 10^{-7}$ m^2/s and $\mu = 9.31 \times 10^{-4}$ N s/m^2. Given that the microstructure of a monolayer is sensitive to the spreading technique [30], well-established methods were employed to obtain films of reproducible surface pressure (see Ref. [22] for details). The monolayers were sheared in a precision-made knife-edge flow apparatus. A precision-bore glass tube of inner diameter $2aA_R = 50.0$ mm was cut to a height of $aA_H = 25.40$ mm and bonded to an optical glass floor to form the cylindrical dish. Two different precision-machined stainless tubes were utilized as knife edges, one with an outer diameter of $2a = 25.40$ mm and the other $2a = 9.53$ mm. The knife edges had very different thicknesses, the larger knife edge had a thickness ratio $\epsilon = 0.02$ and the smaller one had $\epsilon = 0.167$. The two different knife edges were driven over a wide range of rotation rates.

Interfacial velocity field measurements were made primarily using particle tracking velocimetry since it could capture the entire interface, from the knife edge to the cylinder. Independent measurements using Brewster angle microscopy were made confirming that the seeding particles in particle tracking velocimetry do not affect the flow. Experimental details, including how the monolayer was prepared before the knife edge was lowered and its rotation initiated, are provided in the Supplemental Material [26].

Figure 2 shows the radial profiles of azimuthal interfacial velocity from the new nonlinear model (black lines), which were computed using a single combination of the three material properties with dimensionless parameter values of $K = 700$, $n = 7/16$, and Bo (Bo = 10 and Bo = 3.75, since Bo is scaled with the knife-edge radius). These predictions show excellent agreement with the measured profiles (symbols) over two decades of Re. The hydrodynamic regimes range from Stokes flow (Re = 1.2) to

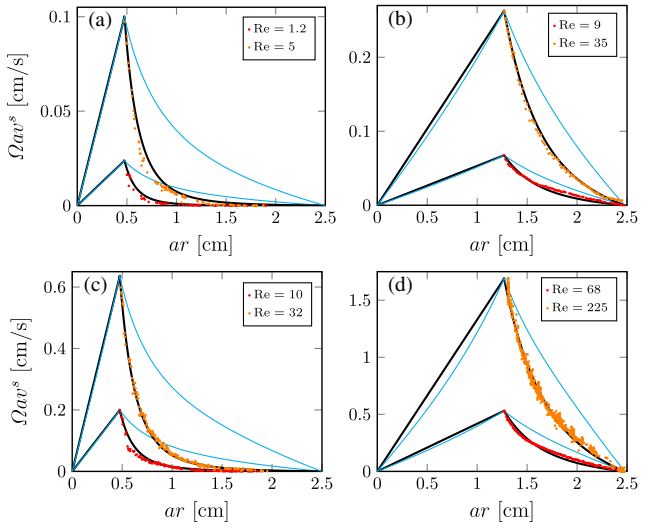

FIG. 2. Radial profiles of the azimuthal velocity at the interface with a DPPC monolayer at surface pressure $\Pi = 40$ mN/m in a knife-edge flow geometry; (a) and (c) are driven by a knife edge of radius $a = 0.47$ cm, (b) and (d) are driven by knife edge of radius $a = 1.27$ cm, at Re as indicated. The symbols correspond to experimental measurements, the thick black lines are the computed velocity profiles with $K = 700$ and $n = 7/16$, and the thin cyan lines are the computed Newtonian profiles ($K = 0$ and $n = 1$), all at the corresponding Re with Bo = 10 for (a) and (c), Bo = 3.75 for (b) and (d).

flows where the inertia of the bulk phase is significant (Re = 225). The shear-rate distribution measured for the two knife edges at various Re (presented in Fig. 2 of the Supplemental Material [26]) shows that the locally imposed shear varies by over six decades.

At the high surface packing of the monolayer employed, the region inside the knife edge rotates essentially as a solid body (not sheared), as seen from the flow profiles computed with the new nonlinear model Eq. (3) for all Re in Figs. 2(a) and 2(c) for the small knife edge ($0 < ar < 0.47$ cm), and in Figs. 2(b) and 2(d) for the large knife edge ($0 < ar < 1.27$ cm). Note that this part of the interface is inaccessible to our interfacial velocity measurements. Only the material between the knife edge and rim of the glass cylinder [$ar > 0.47$ cm in Figs. 2(a) and 2(c) and $ar > 1.27$ cm in Figs. 2(b) and 2(d)] is sheared in this flow geometry, with the shear rate being largest in the vicinity of the knife edge. Previously, we have shown that a strong flow in the bulk phase is driven when an interfacial film of finite surface shear viscosity is sheared [22]. The interfacial response in this flow geometry only decouples from the flow in the bulk phase in the Stokes flow limit or for a film of infinite surface shear viscosity [27].

Computations with the Newtonian model (cyan curves) for flow in the inner region of the small knife edge [$A_R = 5.25$, Figs. 2(a) and 2(c)], using an estimated surface shear viscosity (Bo = 10), capture the solid-body behavior for all Re. However, the Newtonian model with the same estimate of surface shear viscosity (corresponding to Bo = 3.75) for the large knife edge [Figs. 2(b) and 2(d)], predicts flows slower than solid-body behavior in the inner region. This is due to viscous coupling between the bulk and interfacial flows at finite surface viscosity and bulk flow inertia.

The surface velocity profiles predicted using the Newtonian interfacial model with the same estimated surface shear viscosity are significantly faster on the outer knife edge region than both the measured interfacial velocity profiles (symbols) and predictions using the new non-Newtonian model Eq. (3) (thick black curves) across all Re for both knife edges. The slower flows in the outer regions indicate that the effective viscosity of the interfacial films decreases when they are subject to large shear rates. Also, at higher rotation rates (Re = 225), the large knife edge drives a stronger bulk flow. The interfacial response in these regimes is strongly coupled to the driven bulk phase flow. This bulk phase flow inertia also manifests in the deviation between the predicted profiles of the Newtonian model and the new non-Newtonian model. The departure, which is greatest in the outer regions, grows with increasing Re, with maximum deviation occurring for Re = 225 [Fig. 2(d)].

The departures in the velocity profiles at the interface are critical to interpreting rheology. An estimate of shear rate near a knife edge, or any other shearing probe, from the profiles predicted by the Newtonian model is traditionally used to calculate the local material response function (torque or drag coefficient) and in turn used to determine the surface viscosity. The departures described are currently accommodated with an iterated estimate of the viscosity that minimizes the differences between the applied and measured stresses [15]. As shown, the departures are a strong function of the rotation rate and the size of the shearing probe, requiring the iterative estimate to be tailored for the imposed shear-rate distribution (Re). With the new non-Newtonian model, the local shear rate is accurately predicted, eliminating the need for iteration or the velocity profile correction algorithms currently employed [15].

The experimental velocity profiles presented in Fig. 2 were used to determine the effective viscosity across the range of imposed shear rates, and the results are shown in Fig. 3. For each Re, the associated shear-rate distribution was used in Eq. (3) to determine the effective viscosity with $\tilde{K} = 7.4 \times 10^{-4}$ N s$^{-9/16}$ m, $n = 7/16$, and $\mu^s_\infty = 4.2 \times 10^{-5}$ N s/m computed from the dimensionless material parameters used for prediction: K, n, and Bo, respectively. The results show that DPPC films at high surface packing exhibit shear-thinning behavior across the range of imposed shear rates. This is consistent with recent measurements of $\mu^s_{\text{eff}}(\dot{\gamma})$ for DPPC at $\Pi = 40$ mN/m in a double-wall ring viscometer [21], which are included in Fig. 3 as green diamonds. However, the new non-Newtonian model Eq. (3) and the experimentally measured surface velocity profiles shed new insight into the behavior of DPPC films across a hitherto unexplored range of shear rates and flow conditions that are physiologically relevant. In particular, our results indicate that even at low shear rates, such as those experienced in the terminal bronchioles $\dot{\gamma} \sim 10^{-3}$ s^{-1} [31], the power-law behavior persists. Our study confirms and quantifies that condensed-phase DPPC films possess viscosities that are 3–4 orders of magnitude larger than highly fluid films at low surface packing. The measured

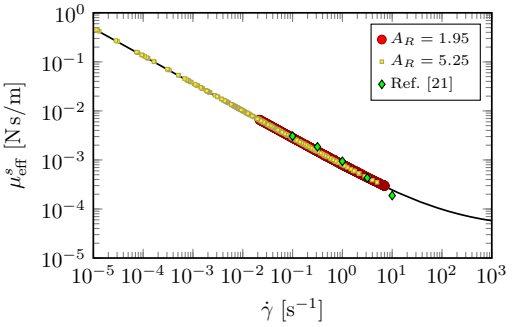

FIG. 3. Effective measured viscosity of DPPC monolayer at surface pressure $\Pi = 40$ mN/m, determined from the experimental interfacial velocity profiles shown in Fig. 2. The black curve is $\mu^s_{\text{eff}} = \mu^s_\infty + \tilde{K}|\dot{\gamma}|^{n-1}$ [Eq. (3)] with $\tilde{K} = 7.4 \times 10^{-4}$ N s$^{-9/16}$ m, $n = 7/16$, and $\mu^s_\infty = 4.2 \times 10^{-5}$ N s/m. Also included are data from Ref. [21], taken in a double-wall ring apparatus with DPPC at $\Pi = 40$ mN/m.

high viscosity is consistent with the required rigid nature of the "squeezed-out" monolayer of DPPC, which is critical to the functioning of lung surfactant [32]. The non-Newtonian model predicts that the response of densely packed shear-thinning films transitions to purely Newtonian behavior at very high shear rates ($\dot{\gamma} \gtrsim 10^4\ \mathrm{s}^{-1}$). The film viscosity in this high-shear limit is $\mu^s_\infty = 4.2 \times 10^{-5}$ N s/m, as indicated by the large-$\dot{\gamma}$ asymptote in Fig. 3.

In conclusion, the new constitutive equation establishes non-Newtonian material properties $\tilde{K}$, n, and μ^s_∞ that accurately predict the nonlinear response of DPPC monolayers under steady shear across a wide range of flow conditions, including hydrodynamic regimes where the inertia of the bulk phase can significantly contribute to the coupled interfacial response. This is especially important when predicting the behavior of soft matter during high-shear events in the body, such as coughing, during which $\dot{\gamma} \gtrsim 10^3\ \mathrm{s}^{-1}$ [33]. Measuring the interfacial velocity profile and matching it to computations from a nonlinear model allows us to explore global or macroscopic effects and quantify interfacial material properties, as opposed to the current practice of using an estimate of the shear rate in the vicinity of the shearing probe to measure torque and determine rheological properties. In contrast to previously reported interfacial rheological models [34], knowledge of the structural distribution of material at the interface is not required to predict the flow behavior. The coupled flow predictions and experiments indicate that the nonlinear behavior of such sheared films does not stem purely from the bulk phase stresses, but that the nonlinear response is due to the inherent non-Newtonian nature of the material at the interface. Across six decades of imposed shear rates (using a combination of varying rotation rates and size of the shearing probe) in the knife-edge flow geometry, the new model shows excellent agreement to measurements covering more than two decades of Re. The non-Newtonian constitutive equation is versatile enough to be generalized for DPPC films at other thermodynamic states to capture linear and nonlinear responses. The framework of assigning a certain functional form to the effective viscosity may also be extended to predict the nonlinear behavior of other soft matter assemblies at fluid-fluid interfaces. In systems involving unsteady flows, appropriate interfacial constitutive equations would be used, including features such as an elastic modulus.

This work was supported NASA Grant No. NNX13AQ22G.

*jmlopez@asu.edu

[1] L. M. C. Sagis, Rev. Mod. Phys. **83**, 1367 (2011).
[2] R. H. Notter, *Lung Surfactants: Basic Science and Clinical Applications* (Marcel Dekker, New York, NY, 2000) DOI: 10.1201/9781482270426.
[3] G. Espinosa, I. López-Montero, F. Monroy, and D. Langevin, Proc. Natl. Acad. Sci. U.S.A. **108**, 6008 (2011).
[4] J. Pelipenko, J. Kristl, R. Rosic, S. Baumgartner, and P. Kocbek, Acta Pharm. **62**, 123 (2012).
[5] L. M. C. Sagis and E. Scholten, Trends Food Sci. Technol. **37**, 59 (2014).
[6] P. J. Beltramo, M. Gupta, A. Alicke, I. Liascukiene, D. Z. Gunes, C. N. Baroud, and J. Vermant, Proc. Natl. Acad. Sci. U.S.A. **114**, 10373 (2017).
[7] K. H. Kim, S. Q. Choi, A. Zasadzinski, and T. M. Squires, Soft Matter **7**, 7782 (2011).
[8] S. Q. Choi, S. Steltenkamp, J. A. Zasadzinski, and T. M. Squires, Nat. Commun. **2**, 312 (2011).
[9] T. Verwijlen, P. Moldenaers, H. A. Stone, and J. Vermant, Langmuir **27**, 9345 (2011).
[10] P. A. Rühs, L. Böni, G. G. Fuller, R. F. Inglis, and P. Fischer, PLoS One **8**, e78524 (2013).
[11] L. M. C. Sagis and P. Fischer, Curr. Opin. Colloid Interface Sci. **19**, 520 (2014).
[12] V. Sharma, A. Jaishankar, Y.-C. Wang, and G. H. McKinley, Soft Matter **7**, 5150 (2011).
[13] A. Jaishankar, V. Sharma, and G. H. McKinley, Soft Matter **7**, 7623 (2011).
[14] L. E. Scriven, Chem. Eng. Sci. **12**, 98 (1960).
[15] S. Vandebril, A. Franck, G. G. Fuller, P. Moldnaers, and J. Vermant, Rheol. Acta **49**, 131 (2010).
[16] J. Ding, H. E. Warriner, J. A. Zasadzinski, and D. K. Schwartz, Langmuir **18**, 2800 (2002).
[17] H. Lodish, A. Berk, C. A. Kaiser, A. Bretscher, H. Ploegh, A. Amon and K. C. Martin, *Molecular Cell Biology*, 6th ed. (W. H. Freeman, Macmillan Learning, New York NY, 2016), ISBN-13:978-1-464641-8339-3.
[18] C. Stefaniu, G. Brezesinski, and H. Moehwald, Adv. Colloid Interface Sci. **208**, 197 (2014).
[19] D. Marsh, Chem. Phys. Lipids **144**, 146 (2006).
[20] A. H. Sadoughi, J. M. Lopez, and A. H. Hirsa, Phys. Fluids **25**, 032107 (2013).
[21] E. Hermans and J. Vermant, Soft Matter **10**, 175 (2014).
[22] A. Raghunandan, J. M. Lopez, and A. H. Hirsa, J. Fluid Mech. **785**, 283 (2015).
[23] A. W. Sisko, Ind. Eng. Chem. **50**, 1789 (1958).
[24] J. C. Slattery, L. M. C. Sagis, and E.-S. Oh, *Interfacial Transport Phenomena*, 2nd ed. (Springer, New York, 2007), DOI: 10.1007/978-0-387-38442-9.
[25] P. T. Underhill, A. H. Hirsa, and J. M. Lopez, J. Fluid Mech. **814**, 5 (2017).
[26] See Supplemental Material at http://link.aps.org/supplemental/10.1103/PhysRevLett.121.164502 for the Supplemental Material contains details of the numerics involved in solving the model equations, experimental details, including how the monolayer was prepared before the knife edge was lowered and its rotation initiated, and the shear-rate distribution measured for the two knife edges at various Re.
[27] J. M. Lopez and A. H. Hirsa, Phys. Fluids **27**, 042102 (2015).
[28] G. L. Gaines, *Insoluble Monolayers at Liquid-Gas Interfaces* (Interscience Publishers, New York, 1966).
[29] J. M. Lopez, M. J. Vogel, and A. H. Hirsa, Phys. Rev. E **70**, 056308 (2004).

[30] H. M. Mansour and G. Zografi, Langmuir **23**, 3809 (2007).
[31] R. Banerjee, J. R. Bellare, and R. R. Puniyani, Biochem. Eng. J. **7**, 195 (2001).
[32] C. Alonso, A. Waring, and J. A. Zasadzinski, Biophys. J. **89**, 266 (2005).
[33] E. S. Vasquez, J. Bowser, C. Swiderski, K. B. Walters, and S. Kundu, RSC Adv. **4**, 34780 (2014).
[34] J. Ding, H. E. Warriner, and J. A. Zasadzinski, Phys. Rev. Lett. **88**, 168102 (2002).